LA-UR-23-24769

Approved for public release; distribution is unlimited.

Title: Development of bubble evolution model for new mechanistic transient fission gas release capability in BISON

Author(s): Cooper, Michael William Donald
Matthews, Christopher
Andersson, Anders David Ragnar

Intended for: Report

Issued: 2024-02-25 (rev.1)

Development of bubble evolution model for new mechanistic transient fission gas release capability in BISON

M. W. D. Cooper, C. Matthews, and D. A. Andersson

Materials Science and Technology Division, Los Alamos National Laboratory

April 30th, 2023

Executive Summary

This report summarizes efforts within NEAMS to investigate the mechanisms that govern fission gas behavior in UO_2. In particular, the focus is on understanding how fission gas behavior causes transient fission gas release and fragmentation/pulverization of high burnup structure (HBS) in UO_2. HBS forms in the periphery of the pellet where temperatures are relatively low. Previously, MD simulations were performed to determine the reaction energies for various Xe and U defects with bubbles, as a function of Xe to vacancy ratio or, equivalently, pressure. As had been shown in FY22 [1], it was found that the unmodified version of the Simple Integrated Fission Gas Release and Swelling (SIFGRS) model within BISON greatly over-predicted the number gas atoms per vacancy in the bubbles in the outer rim of the pellet (a ratio of >1 million). This was due to slow grain boundary vacancy diffusivity and not accounting for the pressure-dependent reaction energy for Xe interstitials with bubbles. The application of the pressure dependent reaction energies was able to restrict Xe to vacancy ratios to 2:1, which is far more realistic than those originally obtained from SIFGRS.

Using new atomic scale insight, SIFGRS has been updated in this work to better capture the physics of bubble pressure evolution throughout the pellet but with a particular emphasis on mechanisms that are important in the cooler periphery of the pellet. Modifications to SIFGRS have been made to account for i) the number of (or lack of) vacancies that arrive along with each Xe atom with pressure dependent reactions energies, ii) a new equation of state from Yang and Wirth [2], iii) a better description of bubble volume based only on the number of vacancies per bubble, and iv) the use of a fracture threshold for grain boundary bubbles [3] allowing bubble growth through micro-cracking. Currently, dislocation punching has been omitted, as in the colder region of the fuel, where significant bubble overpressurization occurs, dislocation creep rates are extremely low and it is unlikely the kinetics of dislocation punching are sufficiently high. However, this assumption will be explored in more detail in the future.

Following implementation of the new equation of state and updates to the definition of bubble volume, bubble pressures were still extremely high in the outer region of the pellet: on the order of 100 GPa. It is unfeasible that such high pressure can occur without the bubble fracturing the grain boundary. Therefore, a fracture threshold derived from MD simulations [3] was implemented. The bubble volume was assumed to immediately increase in response to the bubble pressure exceeding this threshold. This gave reasonable pressure predictions under steady state.

The model was tested under a temperature transient showing an increase in bubble radius in response to the increase in bubble pressure. The increase in bubble radius (assuming the bubble shape does not change) was not sufficient for interconnection. However, if the same volume was assigned to cylindrical cracks of radius 10 nm (an assumption to be tested later) they would be long enough to interconnect. A path forward to test these assumptions and implement a model that allows cracks to grow and shrink has been proposed for future work.

Contents

List of Figures

1 Introduction

For decades, UO_2 has been the dominant fuel material used in commercial light water reactors (LWRs). In an effort to improve economics, LWR operators are attempting to extend the burnup of UO_2 fuel. However, the fuel experiences extreme irradiation damage and accumulation of fission products, resulting in significant microstructural changes during burnup. Limited annealing of radiation-induced defects and limited fission product release at the low temperatures in the periphery of the pellet, lead UO_2 to undergo a restructuring forming the so-called high burnup structure (HBS), characterized by a reduction in grain size and the formation of micron-sized bubbles [4–10]. The reduction in grain size is due to the formation of two types of sub-grains, as identified by Lozano et al. [11]: i) polyhedral grains (0.8 μm) and ii) round grains associated with pores or large bubbles (0.1 μm). Coarsening of fission gas bubbles to micron-sizes is typical of HBS and has been widely observed [5–8, 12]. In addition to the the large bubbles, in some studies sub-grain boundaries were found to be decorated with nm-sized bubbles [4, 8]. Sonoda et al. [8] used TEM to observe such bubbles at sub-grain boundaries in the range of 3.5-8 nm in size.

The formation of HBS creates a number of uncertainties for fuel performance and reactor operations as the material properties are dependent on the microstructural changes. For example, thermal conductivity of the fuel has been measured to recover as a results of HBS formation [13], which has been attributed to a drop in Xe concentrations within the lattice [14, 15]. Another key impact of HBS on fuel behavior, and by far the most important for extended burnups, is the fragmentation and pulverization of the HBS regions of the pellet during transient conditions [16]. Although associated with the formation of HBS, pulverization has also been seen to occur elsewhere. Pulverization, as a opposed to fragmentation, has been defined as disintegration to mostly micron-size particles. Alternatively, fragmentation results in particles of >1 mm. In the review of experiments carried out under the NFIR program, Turnbull et al. [16] showed that pulverization typically resulted in particles of 20-200 μm in size. They defined pulverization thresholds for the local burnup of 71 MWd/kgU (related to the onset of HBS formation) and peak transient temperature of 918 K (related to the fracture mechanism itself). It was suggested by Turnbull et al. [16] that, during the temperature ramp, the expansion of over-pressurized bubbles causes fragmentation/pulverization.

In studies of mechanisms that govern a range of nuclear fuel performance behavior, atomic scale simulations have proven a useful tool. Much of the atomic scale work done on UO_2 has focused on intrinsic and irradiation-enhanced fission gas diffusion [17–25]. Other fission gas behaviors that have been investigated include molecular dynamics (MD) simulations of resolution from bubbles under irradiation [26–28], bubble formation [29, 30], and enhanced Xe diffusion and nucleation of bubbles at dislocations [31]. A cluster dynamics framework that accurately captures irradiation-enhanced U and Xe diffusion in UO_2 has been developed by Matthews et al. [32, 33] by considering a wide range of U and Xe defects. In particular, the diffusion of

mobile bound anti-Schottky trios had to be included. In a previous milestone [34] it was shown, using cluster dynamics, that the irradiation-enhanced diffusion of bound anti-Schottky trios was able to significantly over-pressurize bubbles at low temperatures, such as those in the periphery of the pellet, where HBS forms. For a project funded by EPRI [35], we used MD simulations to examine the impact of nm-size inter-granular bubbles (similar to those observed by Sonoda et al. [8]) on the fracture stress of grain boundaries. It was found that bubbles with similar pressures to those predicted by cluster dynamics in FY20 under NEAMS, caused a significant degradation in grain boundary strength. This was due to the stresses imparted by the bubbles on the grain boundaries when exposed to a temperature ramp. In an FY21 milestone for NEAMS [36], the interaction of Xe-containing defects with bubbles as a function of bubble pressure was determined and implemented in the cluster dynamics code Centipede that was developed to simulate irradiation-enhanced diffusion in UO_2 [32, 33]. It was found that intra-granular bubble over-pressurization resulted in higher U interstitial concentrations, which, through recombination with vacancies and kick-out of Xe substitutional defect, increased the Xe interstitial concentrations to such an extent that Xe interstitial diffusion was dominant at low temperatures. In summary it was shown that Xe diffuses via a i) thermal equilibrium di-vacancy mechanism at high temperature, ii) irradiation-enhanced tetra-vacancy mechanism at intermediate temperature, and iii) interstitial diffusion at low temperatures. In FY22, the reaction energies for specific defects with bubbles (as a function of bubble Xe-vacancy ratio) were implemented in the SIFGRS model in BISON. It was found that Xe interstitials still drive bubble over-pressurization in the cooler outer region of the pellet, however the pressure dependent reaction energy ensured that the number of Xe per vacancy did not exceed 2. This is a far more physical number than that obtained previously; however, it is still expected that other pressure relief mechanisms would activate before that. For example, the micro-cracking threshold studied using MD in another milestone last year [3], which is also thought to be the mechanism responsible for transient fission gas release and, if dramatic enough, pulverization. Dislocation punching could be an active pressure relief mechanism; however, the low temperatures where overpressurization occurs means that dislocation creep rates are very low. Emission of interstitials and dislocation punching was seen as a pressure relief mechanism by Yang and Wirth [2] in MD simulations, even at low temperature, but only for Xe to vacancy ratios of greater than 3:2.

In this work, we implement in SIFGRS new atomic scale data for the equation of state for Xe in UO_2 derived by Yang and Wirth [2] and the MD-informed grain boundary bubble fracture threshold from Galvin et al. [3]. Additionally, we explore an alternative formulation of the flux for the vacancies to the bubbles due to deviations from the equilibrium bubble pressure. The results are discussed in the context of bubble pressure and size evolution under steady-state and a temperature transient.

2 Methods

2.1 General BISON details

To test changes to the fission gas behavior model accounting for insight from the atomic scale, a BISON simulation of the IFA-677.1R5 Halden test was selected [37]. This test was selected as the temperature profiles are similar to that in a LWR and because on-line measurements of pressure, centerline temperature, and fission gas release were taken that can be later used to validate the model. The test was carried out on Rod 5 containing doped UO_2 fuel pellets, irradiated between January 2011 and May 2015 in the Halden Reactor [37]. The specifications of the fuel performance simulations carried out in BISON are shown in Table 2.1. Figure 2.1 shows the applied average linear heating rates, where a) is the true linear heat rate of the IFA-677.1R5 Halden test and b) is a simplified constant linear heat rate that was used to test modifications to the Simple Integrated Fission Gas Release and Swelling (SIFGRS) model.

Table 2.1: Fabrication characteristics of IFA-667.1 rod 5 simulated in this work [37].

	IFA-716.1 Rod 1
Cladding material	Zircaloy-4
Fuel material	UO_2+Cr_2O_3+Al_2O_3
Fill gas	He
Total active fuel stack length (mm)	403.5
Drilled active section length, top (mm)	111.0
Drilled active section length, bottom (mm)	111.1
Pellet inner diameter, drilled sections (mm)	1.8
Pellet outer diameter (mm)	9.13
Diametral gap (μm)	170
Cladding thickness (mm)	0.725
Cladding outer diameter (mm)	10.75
Free volume (cm^3)	5.26
Fill gas pressure (MPa)	1.35
Fuel Cr_2O_3 content (ppm)	500
Fuel Al_2O_3 content (ppm)	200
Fuel U-235 enrichment (%)	4.91
Initial fuel density (kg/m^3)	10700
Fuel average grain radius (μm)	22.5

Due to the small concentration of chromia dopant in UO_2 fuel, many standard undoped UO_2 properties are expected to be readily transferable to doped UO_2. Arborelius et al. measured the thermal diffusivity of fresh fuel, noting only a small change due to doping [38]. It is expected that this small difference will become negligible after some burnup, as the degradation in thermal

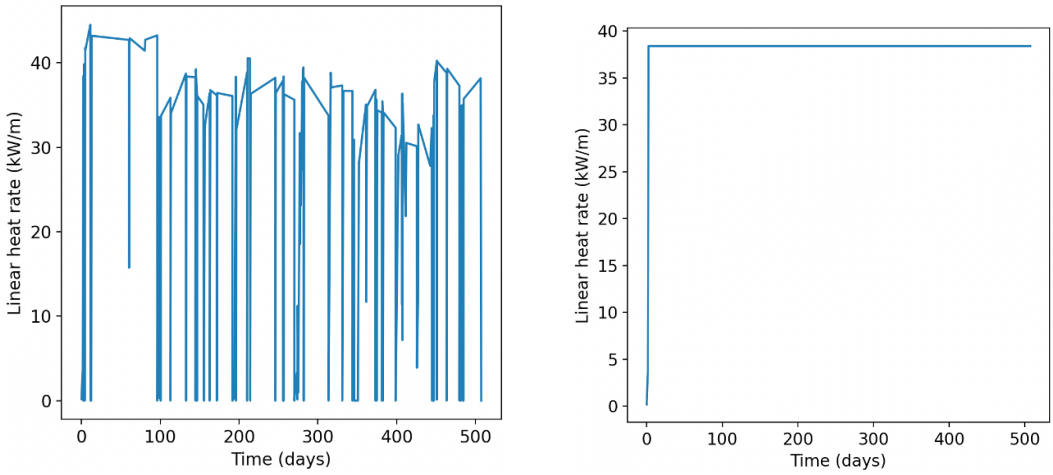

(a) IFA-677.1r5

(b) Simplified

Figure 2.1: The power profiles used in BISON when testing the modifications to the SIFGRS model.

conductivity will be dominated by the accumulation of fission products and irradiation induced defects. The larger grain size of doped UO_2 is expected to have a negligible effect on thermal transport, given that molecular dynamics (MD) simulations indicate grain size must be on the sub-micron scale to have a noticeable impact [39]. Therefore, the Halden thermal conductivity correlation for undoped UO_2, as a function of burnup (as documented in [40, 41]), is used for simulations of the Halden tests in this study. The specific heat capacity of doped UO_2 has been noted to be within 3% of that for undoped UO_2 [38]. As such, we have applied the Fink data for undoped UO_2 [42] to doped UO_2. Arborelius et al. note that Cr+Al doped UO_2 has the same thermal expansion as undoped UO_2 [38]. Therefore, the standard BISON UO_2 thermal strain model [43] will be adopted here for Cr-doped UO_2. In BISON, the grain growth of standard UO_2 due to the high temperatures experienced in-reactor is described by the model from Ainscough et al. [44]. Although this model is also applied here for doped UO_2, it does not result in significant grain growth due to the large initial grain diameter of doped UO_2 (40-70 μm). This behavior is expected due to the stability of the large grains. During irradiation, nuclear fuel undergoes further densification beyond the beginning of life sintered density. Observations during the Halden Reactor Project [45] showed that a densification of 0.1-0.2% occurred for Cr-doped UO_2 fuel rods. Therefore, the standard UO_2 densification ESCORE model [46] was used for doped UO_2 but with the maximum densification set to 0.15% in the simulations of the Halden tests. Densification information is not available for the Framatome ramps test, hence the standard value of 1% for undoped UO_2 is applied to doped UO_2. Such small additions of dopant are not expected to influence the uncracked elastic behavior and, as such, typical elastic constants for standard UO_2 are applied. Larger grains can reduce the fracture strength of UO_2 [47]. However, in the absence of a specific model for Cr-doped UO_2, the isotropic softening model for fuel cracking from Barani et al. for undoped UO_2 is used [48]. The creep rate is treated using the MATPRO correlations for standard UO_2 [43]. A creep model has not yet been implemented for doped UO_2 but is being developed in a separate milestone.

2.2 Intra-granular fission gas behavior

The fission gas behavior model for oxide fuel in BISON [49] incorporates the fundamental physical mechanisms for fission gas release (FGR) [40,50]. The diffusion of fission gas from the bulk to grain boundaries is governed by the unperturbed diffusivity of single gas atoms through the UO_2 lattice (D), trapping at intra-granular bubbles (g), and resolution from intra-granular bubbles (b). Transport from within a spherical grain (as assumed in this model [50]) to the grain boundary can be described by:

$$\frac{\partial C_{ig}}{\partial t} = \frac{b}{b+g} D \nabla^2 C_{ig} + \beta \tag{2.1}$$

where C_{ig} (atoms·m^{-3}) is the intra-granular gas concentration, g (s^{-1}) is the trapping rate, b (s^{-1}) is the resolution rate, D (m^{2}s^{-1}) is the unperturbed diffusivity, and β (atoms·s^{-1}) is the source term for the generation of gas atoms through fission. The effective diffusivity can be described as [51]:

$$D_{\text{eff}} = D \frac{b}{b+g} \tag{2.2}$$

The trapping and resolution parameters, g [52] and b [53], are given by:

$$g = 4\pi RND \tag{2.3}$$

$$b = 3.03 \dot{F} \pi l_f (R + Z_0) \tag{2.4}$$

where $l_f = 6 \times 10^{-6}$ m is the length of a fission fragment track, $Z_0 = 10^{-9}$ m is the radius of influence of a fission fragment [53], and $\dot{F}$ is the fission rate density. The bubble radius and bubble density, R and N respectively, are solved for during the BISON simulations using the model described by Pizzocri et al. [54].

The fission gas diffusivity for doped UO_2 is given by a lower length scale informed model derived by Cooper et al. [55] as an enhancement to the empirical undoped UO_2 model of Turnbull et al. [56, 57]. The model accounts for the impact of doping, fission rate and temperature.

2.3 Unmodified inter-granular bubble model (SIFGRS)

The SIFGRS model accounts for the evolution of inter-granular bubbles, the associated gaseous fuel swelling, and the eventual saturation of the grain boundaries, resulting in FGR to the fuel rod free volume. Swelling due to intra-granular bubbles is not considered in the present work, as it is generally less important than that due to inter-granular bubbles in UO_2 under normal operating conditions, at least for burnups below 45 GWd/t [58]. A detailed description of the fission gas model can be found in [40,50,59]. Here we describe some key features of the model, paying particular attention to components of the model that we will modify to account for low temperature irradiation-enhanced defect processes that cause bubble over-pressurization.

As Eq. (2.1) is solved, the number of Xe atoms arriving at the grain boundaries is determined for each time step. By assuming all Xe atoms arriving at the grain boundary are accommodated

immediately within inter-granular bubbles, the rate of change of gas atoms per bubble, $\frac{dn_{Xe}}{dt}$, is calculated. When defining the bubble pressure in SIFGRS, it is assumed that Xe arrives as single atoms, or interstitials (i.e., unaccompanied by vacancies). Therefore, for the pressure of the bubbles to be relieved, vacancies must diffuse along grain boundaries to the bubbles. The rate of arrival of vacancies at the bubbles, based on the model of Speight and Beere [60] for the growth of grain boundary voids under an applied tensile load, is given by:

$$\frac{dn_v}{dt} = \frac{2\pi[v]D_v\delta_g}{k_BTS}(p - p_{eq}) \tag{2.5}$$

n_v = number of vacancies per grain-face bubble
t = time (s)
$[v]$ = vacancy concentration in the grain boundary (per site)
D_v = vacancy diffusivity in grain boundaries ($m^{-2}s^{-1}$)
k_B = Boltzmann constant (JK^{-1})
T = temperature (K)
p = bubble pressure (Pa)
p_{eq} = equilibrium bubble pressure (Pa)
The bubble volume is described by:

$$V_{bubble} = b_{Xe}n_{Xe} + \Omega_v n_v \tag{2.6}$$

Ω_v = volume per vacancy (m^3)
b_{Xe} = the atomic volume of Xe from the van der Waals constant (m^{-3})
n_{Xe} = number of gas atoms per grain-face bubble as determined by solving Eq. (2.1) for the intra-granular behavior.

This treatment of the bubble volume, in Eq. (2.6), effectively assumes that gas atoms, as well as vacancies, contribute to the free space that makes up a void/bubble. This assumption is questionable and will be probed in this work.

The pressure of a bubble, p, in BISON is in theory determined from the simple (excluding the a gas constant) van der Waals equation of state:

$$p = \frac{n_{Xe}k_BT}{V_{bubble} - bn_{Xe}} \tag{2.7}$$

A consequence of combining Eqs. (2.6) and (2.7) is that the equation governing the pressure of a bubble reverts to the ideal gas law:

$$p = \frac{k_BT}{\Omega_v}\frac{n_{Xe}}{n_v} \tag{2.8}$$

The equilibrium bubble pressure, which, when combined with p, provides the driving force for bubble swelling, is given by:

$$p_{eq} = \frac{2\gamma}{R_{gf}} - \sigma_h \tag{2.9}$$

p_{eq} = equilibrium bubble pressure (Pa)

$\gamma =$ surface tension (Jm^{-2})
$R_{gf} =$ radius of curvature of grain-face bubbles (m)
$\sigma_h =$ hydrostatic stress (one third of the trace of the stress tensor) (Pa)

In summary, the arrival of gas from the grain raises inter-granular bubble pressures (see Eq. (2.8)), increasing the driving force for vacancies to diffuse to inter-granular bubbles via grain boundary diffusion (see Eq. (2.5)).

2.4 Lower-Length-Scale informed Modifications to Inter-Granular Bubble Model

2.4.1 Equation of state for fission gas

The original version of SIFGRS uses the simple van der Waals equation of state for Xe to describe the pressure of bubbles in UO_2 as a function of the number Xe atoms and vacancies that comprise the bubble, and the local temperature. This equation performs well for the gas under small to moderate pressures. However, it is possible that extremely high pressure bubbles occur at the low temperatures in the periphery of the pellet where the fuel becomes susceptible to pulverization. Therefore, an equation of state derived from atomic scale simulations by Yang and Wirth [2] has been implemented in BISON. In this equation of state, the pressure of the bubble is given by:

$$p = \rho k_B T \left(1 + B\rho_r + C\rho_r^2 + E\rho_r^4\right) \tag{2.10}$$

where $\rho_r = \rho/\rho_c$ is the reduced gas density and $\rho_c = 5.06\ \mathrm{nm}^{-3}$. Wirth and Yang also derived a radially-dependent term accounting for contrainment by the UO_2 lattice, which has been omitted here, given that it was shown to only be significant for nm-size bubbles (smaller than the bubbles that form at grain boundaries).

B, C, and E are dependent on the reduced temperature $T_r = T/T_c$, where $T_c = 290$ K, such that:

$$B = b_0 + \frac{b_1}{T_r} + \frac{b_2}{T_r^2} \tag{2.11}$$

$$C = c_0 + \frac{c_1}{T_r} + \frac{c_2}{T_r^2} \tag{2.12}$$

$$E = e_0 + \frac{e_1}{T_r} + \frac{e_2}{T_r^2} \tag{2.13}$$

where b_i, c_i, and e_i are fitted constants:
$b_0 = 0.261323$
$b_1 = -1.132763$
$b_2 = 0.028564$
$c_0 = 0.318315$
$c_1 = -0.038613$
$c_2 = -0.248067$
$e_0 = -0.003885$

$e_1 = 0.069736$
$e_2 = 0.18356$

In this work, we treat the only source of free space for the bubbles as being due to vacancies, while fission gas atoms occupy this space increasing ρ and p. We have, therefore, defined the bubble volume as $n_v\Omega_v$ and $\rho = n_{Xe}/(n_v\Omega_v)$.

Using this new version of the equation of state for Xe, the pressure can more accurately be defined for a given T, and n_{Xe}/n_v, which will enable a better description of the driving force for various pressure release mechanisms, such as that described in Eq. (2.5) for fracture.

2.4.2 Revised reaction rates for vacancies with grain boundary bubbles

In this section, we describe an alternative to the linear approximation for the flux of grain boundary vacancies to bubbles to relieve the bubble pressure. A similar approach to that of Matthews et al. [32], which was used to describe the rate of change of bulk vacancy concentrations due to reactions with intra-granular bubbles has been used.

The change in the energy of the bubble due to the addition of a vacancy is accounted for by $dE = -PdV$, where the increase in the bubble volume is equal to the volume of one vacancy, as such:

$$G_0 = -G_{f,v} - (p - p_{eq})\Omega_v \tag{2.14}$$

where G_0 is the reaction energy for a vacancy being incorporated within a bubble of pressure p. $G_{f,v}$ is the formation energy of the vacancy, which controls the equilibrium vacancy concentration in the grain boundary,

$$[v] = \exp\left(\frac{-G_{f,v}}{k_B T}\right) \tag{2.15}$$

The intersect between an intergranular bubble and the grain boundary makes a cylinder with the same radius as the bubble and a height equal to the grain boundary thickness. The surface area that defects can flow through to enter the bubble is, therefore, $A = 2\pi R_{gf}\delta$; whereby $\delta << R_{gf}$. The flux of defects into a grain boundary represents a very similar problem geometrically to that of defects to a dislocation, which is given by [61, 62]:

$$\frac{dc_v}{dt} = \frac{2\pi D_v c_v \rho_d}{\ln\left(\frac{\mathcal{R}_d}{R_d}\right)} \tag{2.16}$$

where R_d is the capture radius and $2\mathcal{R}_d$ is the separation between dislocation cores. ρ_d is the dislocation line density in m/m^3, such that $\rho_d = c_d l_d$, where c_d is the number density of dislocations and l_d is the dislocation length. c_v is the concentration of vacancies. This can written in terms of the rate of vacancies arriving at a single dislocation as:

$$\frac{dn_v}{dt} = \frac{2\pi D_v c_v l_d}{\ln\left(\frac{\mathcal{R}_d}{R_d}\right)} \tag{2.17}$$

Therefore, considering that a bubble intersecting a grain boundary represents fundamentally the same geometric problem as for a dislocation, except that the length over which the grain boundary vacancies and the bubble react is the grain boundary thickness, rather than the dislocation length,

$$\frac{dn_v}{dt} = \frac{2\pi D_v [v] \delta}{\ln\left(\frac{\mathcal{R}}{R_{gf}}\right)} \tag{2.18}$$

However, the above reaction assumes that it is always favorable for bubbles to absorb vacancies, which is only true if the bubble pressure exceeds the equilibrium bubble pressure. Using the same driving force relationship described by Matthews et al., the reaction rate can be written as:

$$\frac{dn_v}{dt} = \frac{2\pi D_v \delta}{\Omega \ln\left(\frac{\mathcal{R}}{R}\right)} \left[[v] - \exp\left(\frac{\Delta G_0}{k_B T}\right) \right] \tag{2.19}$$

By substituting Eq. (2.15) into Eq. (2.19) and assuming that vacancies within the grain boudnary are always at thermal equilibrium one obtains:

$$\frac{dn_v}{dt} = \frac{2\pi [v] D_v \delta}{\Omega \ln\left(\frac{\mathcal{R}}{R}\right)} \left[1 - \exp\left(\frac{(p_{eq} - p)\Omega_v}{k_B T}\right) \right] \tag{2.20}$$

The dependence on inter-granular bubble concentration comes from $\mathcal{R}$, which is the separation between the centers of the bubbles and is calculated within SIFGRS based on the areal density of the bubbles.

2.4.3 MD-derived reaction energies

In a previous milestone [34], the average energy of a Xe atom in a fission gas bubble based on 0 K static atomic scale simulations was found as a function of $\frac{n_{Xe}}{n_v}$, as follows:

$$\begin{aligned} \frac{E_{bubble} - E_{void}}{n_{Xe}} = & A\left(\frac{n_{Xe}}{n_v}\right)^8 + B\left(\frac{n_{Xe}}{n_v}\right)^7 + C\left(\frac{n_{Xe}}{n_v}\right)^6 \\ & + D\left(\frac{n_{Xe}}{n_v}\right)^5 + E\left(\frac{n_{Xe}}{n_v}\right)^4 + F\left(\frac{n_{Xe}}{n_v}\right)^3 + G\left(\frac{n_{Xe}}{n_v}\right)^2 + H\left(\frac{n_{Xe}}{n_v}\right) \end{aligned} \tag{2.21}$$

$A = 0.02210$ eV
$B = -0.3282$ eV
$C = 1.950$ eV
$D = -5.858$ eV
$E = 9.189$ eV
$F = -7.091$ eV
$G = 3.372$ eV
$H = -1.033$ eV where $\frac{n_{Xe}}{n_v}$ is the Xe to vacancy ratio of the bubble. $\frac{E_{bubble} - E_{void}}{n_{Xe}}$ was found to be broadly independent of bubble size, at least for the small bubbles tested, and is only dependent on $\frac{n_{Xe}}{n_v}$, allowing a single polynomial to be fitted for $\frac{E_{bubble} - E_{void}}{n_{Xe}}$ that describes all bubble sizes.

This energy relates to the static mechanical gas-gas and gas-UO_2 interactions, which can become important for extremely large bubble pressure. For example, it has been shown that if interstitial Xe or U atoms arrive at fission gas bubble they will increase the bubble pressure until $\frac{n_{Xe}}{n_v}$ becomes so high that further increases in the bubble energy (as described by Eq. (2.21)) will prevent further incorporation of interstitial defects; thereby, resulting in an upper limit in $\frac{n_{Xe}}{n_v}$. As described in previous milestones the change in the energy of the bubble due to reaction with a given cluster can be combined with the defect energy of that cluster as follows.

By multiplying Eq. (2.21) by n_{Xe} and then differentiating with respect to n_v the change in energy of the bubble due to one vacancy being added was determined.

$$\Delta E_v = \frac{\partial(E_{bubble} - E_{void})}{\partial n_v} = -8A\left(\frac{n_{Xe}}{n_v}\right)^9 - 7B\left(\frac{n_{Xe}}{n_v}\right)^8 - 6C\left(\frac{n_{Xe}}{n_v}\right)^7 - 5D\left(\frac{n_{Xe}}{n_v}\right)^6 - 4E\left(\frac{n_{Xe}}{n_v}\right)^5 - 3F\left(\frac{n_{Xe}}{n_v}\right)^4 - 2G\left(\frac{n_{Xe}}{n_v}\right)^3 - H\left(\frac{n_{Xe}}{n_v}\right)^2 \quad (2.22)$$

Similarly by multiplying Eq. (2.21) by n_{Xe} and then differentiating with respect to n_{Xe}, the change in the energy of a bubble due to the addition of a single Xe atom was determined [36].

$$\Delta E_{Xe} = \frac{\partial(E_{bubble} - E_{void})}{\partial n_{Xe}} = 9A\left(\frac{n_{Xe}}{n_v}\right)^8 + 8B\left(\frac{n_{Xe}}{n_v}\right)^7 + 7C\left(\frac{n_{Xe}}{n_v}\right)^6 + 6D\left(\frac{n_{Xe}}{n_v}\right)^5 + 5E\left(\frac{n_{Xe}}{n_v}\right)^4 + 4F\left(\frac{n_{Xe}}{n_v}\right)^3 + 3G\left(\frac{n_{Xe}}{n_v}\right)^2 + 2H\left(\frac{n_{Xe}}{n_v}\right) \quad (2.23)$$

Therefore, the reaction energy of a defect containing a certain number of Xe atoms and vacancies with a bubble can be expresses as:

$$E_{defect-bubble} = -E_{defect} + (n_{V_U} - n_{U_i})\Delta E_v + n_{Xe}\Delta E_{Xe} \quad (2.24)$$

where E_{defect} is the formation energy of the defect cluster. n_{V_U} is the number of U vacancies in the cluster, n_{U_i} is the number of U interstitials, and n_{Xe} is the number of Xe atoms. For example, if the Xe-containing cluster is $\{Xe : 4V_U : 3V_O\}$, then $n_{V_U} = 4$, $n_{U_i} = 0$, and $n_{Xe} = 1$. By assuming stoichiometric growth of the bubble (assisted by rapid diffusion of oxygen defects), the reaction energy is not sensitive to the number of oxygen vacancies [34]. These $\frac{n_{Xe}}{n_v}$ dependent reaction energies will be used in modifications to SIFGRS to determine reaction rates that account for both the composition of the defect and the bubble pressure.

2.4.4 Accounting for vacancies that assist gas diffusion

At a given temperature, gas can diffuse though the bulk lattice via one of several mechanisms. It was show in previous work, that it diffuses via a i) thermal equilibrium di-vacancy mechanism at high temperature, ii) irradiation-enhanced tetra-vacancy mechanism at intermediate temperature, and iii) interstitial diffusion at low temperatures. Therefore, as gas arrives at inter-granular bubbles it is accompanied by a differing number of vacancies depending on the temperature. This can be seen in Fig. 2.2, where the number of vacancies accompanying each gas atom at a given

temperature is shown. This was based on the relative diffusivities of different Xe-containing defects predicted from cluster dynamics simulations, where the only the most dominant defect were included:

$$n_{\frac{v}{Xe}} = \frac{2D_{Xe_{2U}} + 4D_{Xe_{4U}}}{YD_{Xe_i} + D_{Xe_{2U}} + D_{Xe_{4U}}} \tag{2.25}$$

where $D_{Xe_{4U}}$, $D_{Xe_{2U}}$, and D_{Xe_i} are fitted to the data from [36]. Y accounts for the change in the driving force for Xe interstitial incorporation into inter-granular bubbles as a function of $\frac{n_{Xe}}{n_v}$:

$$Y = \begin{cases} 1 - \exp\left(\frac{\Delta G_{0,Xe_i}}{k_B T}\right), & \text{if } G_{0,Xe_i} < 0, \\ 0, & \text{otherwise} \end{cases} \tag{2.26}$$

where G_{0,Xe_i} is the reaction energy for a Xe interstitial with a bubble as a function of the $\frac{n_{Xe}}{n_v}$ of the bubble, as described by Eqs. (2.23) and (2.24). Analogous Y terms for the Xe_{2U} and Xe_{4U} defects are always one so are not shown in Eq. (2.25).

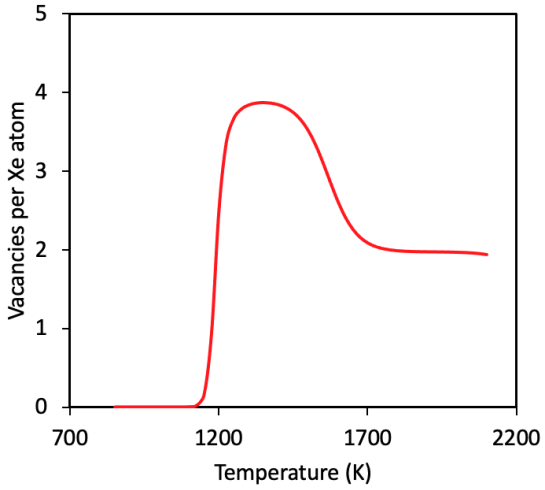

Figure 2.2: The number of vacancies per Xe atom arriving at inter-granular bubbles, $n_{\frac{v}{Xe}}$, based on Centipede simulations where intra-granular bubble pressure is evolved, such that Xe interstitial diffusivity dominates at low temperatures.

The rate of arrival of vacancies by assisting gas diffusion is given as:

$$\frac{dn_v}{dt} = n_{\frac{v}{Xe}} \frac{dn_{Xe}}{dt} \tag{2.27}$$

2.4.5 MD-derived cracking threshold

In a previous milestone [3], MD simulations were performed to examine the pressure at which inter-granular bubbles induce micro-cracking along the grain boundary. The MD simulation supercells contained a grain boundary with a void centered upon it. Bubbles of radius 5 nm

and 20 nm were examined. For a given void radius, gas atoms were inserted, creating a bubble. The number of gas atoms was increased, causing a rise the bubble pressure. Eventually the bubble pressure was sufficient to cause a micro-crack to extend from the grain boundary-bubble intersection. This provided additional volume for the gas, thereby, lowering the bubble pressure and reducing the energy of the system. An MD-informed fracture threshold was defined based on the bubble pressure at which the micro-crack occurred. This is shown in Fig. 2.3, as a function of bubble radius. The following expression was fitted to that data for implementation in BISON:

$$p_{crack} = 2.11 \times 10^5 R_{gf}^{-0.529} \tag{2.28}$$

where p_{crack} is the bubble pressure in Pa at which a crack occurs, as a function of bubble radius, R_{gf}, in m. The simulations used to parameterize this expression were carried out at 600 K. No dislocation punching occurred in these simulations before cracking occurred. Additional simulations are being carried out at different temperatures as part of another work package this FY but until those new simulations are complete this behavior is assumed to be independent of temperature. Having said that, the above is expressed in terms of pressure, which is itself temperature dependent through the equation of state.

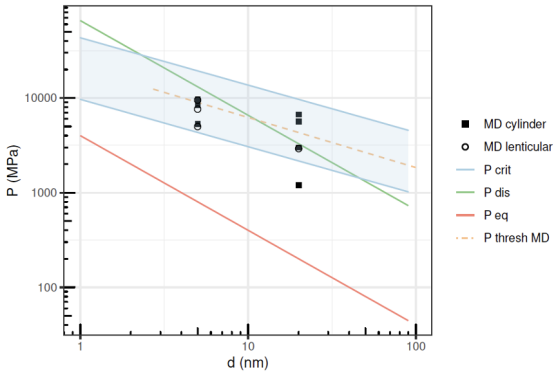

Figure 2.3: A plot showing several pressure thresholds, as a function of bubble radius, that can result in pressure relief from bubbles in UO_2. The red line shows the equilibrium bubble pressure, the green lines shows the dislocation punching threshold based on the experimental shear modulus. The shaded blue band represents the range of cracking thresholds estimates using an analytical expression, while the dashed orange line indicates a fracture threshold derived from molecular dynamics simulations by Galvin et al. [3].

If the pressure of the bubbles (defined by Eq. (2.5)) exceeds the MD-derived fracture threshold given by Eq. (2.28) the volume of the bubble was assumed to immediately increase through cracking to provide the volume required, ΔV, to lower the pressure back to the fracture threshold. We have assumed that, through surface diffusion, cracks that have extended from bubbles are able to rapidly reconfigure so that their volume becomes incorporate into the bubble and the bubble maintains its lenticular shape. In a given time step, the increase in bubble volume due to fracture is defined as:

$$\Delta V = (p - p_{crack}) \frac{dV}{dP} \tag{2.29}$$

where $\frac{dV}{dP}$ is defined using a first order finite difference approach applied to the equation of state described in Section 2.4.1:

$$\frac{dP}{dV} = \frac{p(V) - p(V + \delta V)}{\delta V} \tag{2.30}$$

The change in the number of vacancies per inter-granular bubble is therefore:

$$\Delta n_v = \frac{\Delta V}{\Omega_v} \tag{2.31}$$

whereby, $\frac{dn_v}{dt} = \frac{\Delta n_v}{\Delta t}$ and Δt is the timestep. The reverse of this process is never permitted to occur and Δn_v from Eq. (2.31) can never be negative. The use of Eqs. (2.29) to (2.31) inherently assumes both that cracks can occur immediately in response to the bubble exceeding p_{crack} and that the bubble can immediately return to its ideal lenticular shape. The former assumption is justified given that brittle crack propagation occurs at the speed of sound, which is effectively instantaneous. The latter assumption is based on the fact that surface diffusion occurs much more quickly than the other diffusive processes. The validity of this assumption will be discussed based on the results presented here.

Yang and Wirth also derive a term to account for constraint due to the surrounding lattice. This was shown to only be important for nm-sized bubbles, such as those within the grain, and is omitted here due to the relatively large size of bubbles at the grain boundary (> 50 nm).

2.4.6 Combined modifications

The total rate of change of vacancies in a single bubble due to the various mechanisms discussed above can be expressed as:

$$\frac{dn_v}{dt} = \left(\frac{dn_v}{dt}\right)^{pressure} + \left(\frac{dn_v}{dt}\right)^{Xe} + \left(\frac{dn_v}{dt}\right)^{crack} \tag{2.32}$$

The three terms represent the arrival of vacancies due to bubble-pressure induced diffusion by equilibrium vacancy concentrations, ii) the vacancies that inherently assist Xe diffusion, and iii) the increase in volume due to grain boundary cracking. These processes are, respectively, described by i) Eq. (2.20) or Eq. (2.5), ii) Eq. (2.27), and iii) Eqs. (2.30) and (2.31). In the following section the results of introducing these modifications sequentially along with alterations to the equation of state described in Section 2.4.1 will be discussed.

3 Results and Discussion

3.1 Unmodified SIFGRS

As a baseline, the results of bubble evolution with the unmodified version of SIFGRS are shown. The primary metrics of interest are the bubble size and pressure evolution, as well as the ratio of the number of gas atoms per bubble to the number of vacancies per bubble. These are shown as a function of time for the IFA 677 rodelet case described in Section 2.1. For simplicity and more rapid simulation times, the constant power case was used. Figure 3.1 shows the results as a function of time at three radial positions in the pellet: i) inner position of the pellet (red), ii) mid-way between the pellet center and the periphery of the pellet (green), and iii) the outer edge of the pellet (blue). All positions are located at the axial mid-point of the rodlet.

It can be seen that in the periphery $\frac{n_{Xe}}{n_v}$ greatly exceeds any value that would be considered reasonable. This is due to the immobility of grain boundary vacancies in the cooler periphery of the pellet, see Fig. 3.1d. Conversely the higher temperatures at the mid-point and the inner part of the pellet mean that highly mobile vacancies can relieve the bubble pressure.

The assumption that the bubble volume consists of both the volume of the vacancies and the gas atoms (Eq. (2.6)), when used in the simple van der Waals equation (Eq. (2.7)), returns the ideal gas law (Eq. (2.8)). Hence, bubble pressures in the range of several GPa are obtained, whereas for $\frac{n_{Xe}}{n_v}$ on the order 10 million, far higher pressures would be expected. Before addressing the issue around the assumptions of the bubble volume and gas equation of state, the fact that gas atoms can diffuse by vacancy-assisted mechanisms should be addressed.

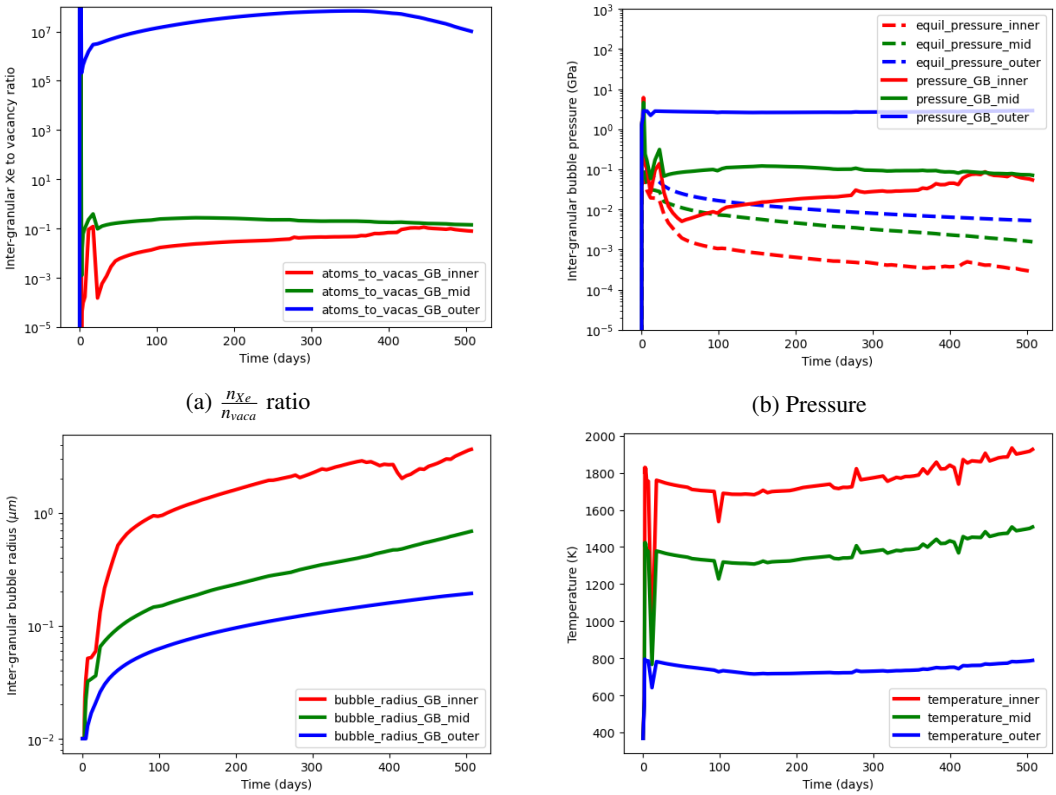

(a) $\frac{n_{Xe}}{n_{vaca}}$ ratio

(b) Pressure

(c) Radius

(d) Temperature

Figure 3.1: Prediction from the unmodified SIFGRS model in BISON for inter-granular bubble behavior at three positions in the fuel pellet for the IFA-677.1R5 case with a constant power applied.

3.2 Including vacancies that assist Xe diffusion

In a previous milestone, we demonstrated that, by accounting for vacancies that assist Xe diffusion and, in particular, the fact that the driving force for Xe interstitials to become incorporated into bubbles tends to zero as the bubble pressure becomes high, n_{Xe}/n_v values should not be greater than 2. This phenomenon has been implemented in SIFGRS and the results are shown here as a benchmark, see Fig. 3.2, against which to see the impact of the new physics implemented this year. Figure 3.2a demonstrates that n_{Xe}/n_v in the center of the pellet and at the radial mid-point are not affected by including the number of vacancies that assist diffusion of a Xe atom (Eq. (2.27)). This is due to to the high operating temperatures at these locations and the correspondingly mobile grain boundary vacancies that dominate pressure relief. On the other hand, n_{Xe}/n_v in the cooler periphery of the pellet saturates at about 2, as had been seen previously. However, the use of the bubble volume assumption in Eq. (2.6) means the van der Waals equation becomes the ideal gas law and results in much lower pressures that would be expected for such a high n_{Xe}/n_v (an average of two atoms occupying the space previously occupied by a single vacancy). Similarly, by accounting for the volume of both the vacancies and the gas atoms in the total bubble volume, it is expected that the bubble radius is overestimated. Both of these things are important, given that intergranular bubble pressure and separation (governed by the size and number density) have been shown to be key characteristics that impact the likelihood for grain boundary fracture during temperature ramps [3]. For comparison, the threshold for micro-cracking around grain boundaries, based on the MD simulations of Galvin et al. [3], is also shown in Fig. 3.2b. Although the bubbles pressures are below the threshold for all of the results shown in this case, changes to bubble equation of state may alter that conclusion.

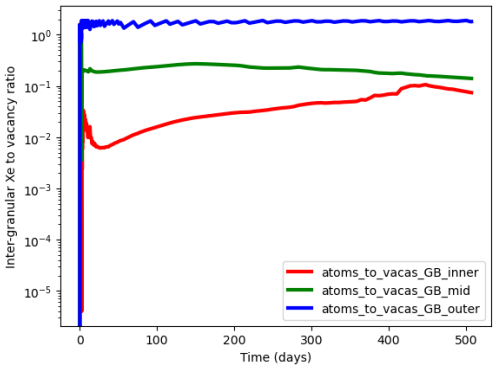

(a) $\frac{n_{Xe}}{n_{vaca}}$ ratio

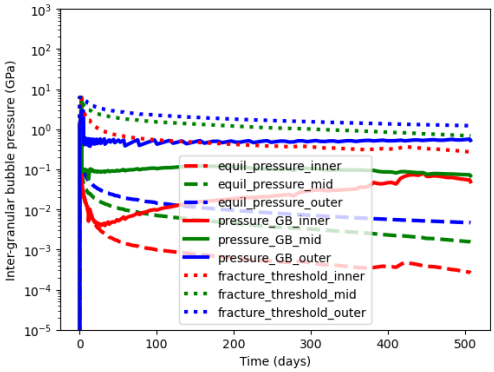

(b) Pressure

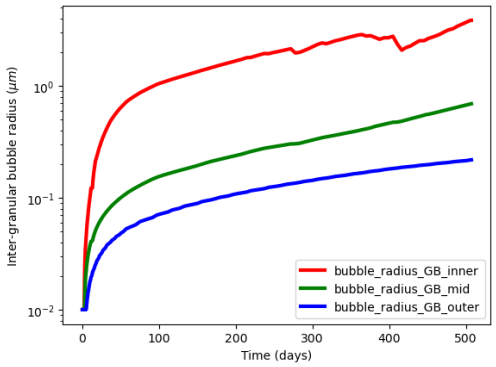

(c) Radius

Figure 3.2: Prediction from the SIFGRS model in BISON for inter-granular bubble behavior at three position in the fuel pellet for the IFA-677.1R5 case with a constant power applied. n_{Xe}/n_v-dependent reaction energies have been applied.

3.3 Updated equation of state and volume

While more physical values for n_{Xe}/n_v were obtained by using MD-informed reactions energies to described the lowering of the driving force for Xe interstitials to continue to increase bubble pressure as n_{Xe}/n_v approaches 2, there remain issues with the predictions of bubble radius and pressure. Both of these are important for later predicting the transient fission gas release and pulverization. Only when high pressure bubbles are near enough to each other (of sufficient size and number density) can the creation of microcracks during a transient be sufficient to interconnect bubbles leading to gas release or grain boundary decohesion.

To address these issues, we have, first, removed the contribution of gas atoms to the free volume of the bubbles. Instead only vacancies can grow bubbles and the gas atoms, instead, occupy this free spaces and increase the pressure. As discussed in Section 2.4.1, the gas density is $n_{Xe}/(\Omega_v n_v)$ and was used in the equation of state derived by Yang and Wirth [2]. By comparing Figs. 3.2a and 3.3a it can be seen that these changes have only a minor impact on n_{Xe}/n_v. However, the impact of replacing the ideal gas law with the equation of state from Wirth and Yang has a profound effect on the bubble pressures in the periphery of the pellet, increasing them from a few hundred MPa to around 100 GPa, see Figs. 3.2b and 3.3b. The new equation of state has a much smaller effect on the pressure of the inner and mid-point bubbles, where the n_{Xe}/n_v remains low and the ideal gas law is expected to perform reasonably well. Comparison of the predicted bubble pressures in the outer region of the pellet with the fracture threshold derived by Galvin et al. clearly shows that fracture of the grain boundary should be active as bubble growth mechanism, even for steady state conditions. This will be addressed in a later section. An interesting point to note is that, due to Xe being in the solid state for such a high n_{Xe}/n_v, the bubble pressure is essentially temperature independent and no further increase in pressure would be seen for a temperature ramp.

As well as updating the equation of state, the new formulation of the bubble volume was applied and, as expected, it resulted in a reduced bubble radius in the outer region of the pellet, see Fig. 3.3c. Only a small impact was seen on the bubble radius in the hotter regions of the pellet (inner and mid), given that, even with the old assumption, the low n_{Xe}/n_v means that the vast majority of the bubble volume in those regions was already accounted for by vacancies rather than atoms.

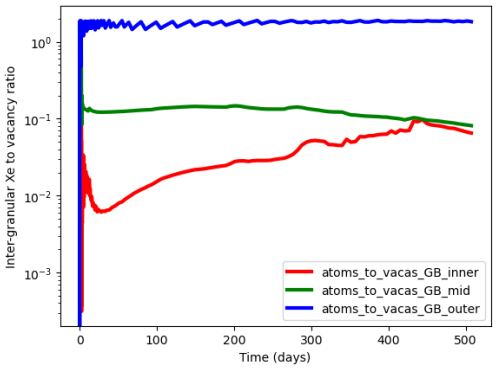

(a) $\frac{n_{Xe}}{n_{vaca}}$ ratio

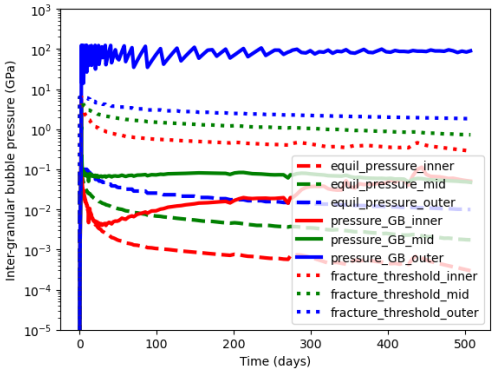

(b) Pressure

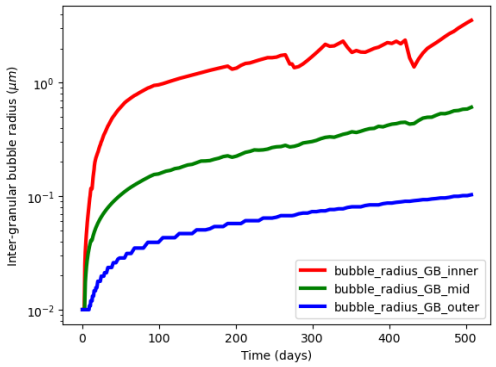

(c) Radius

Figure 3.3: Prediction from the SIFGRS model in BISON for inter-granular bubble behavior at three position in the fuel pellet for the IFA-677.1R5 case with a constant power applied. An updated equation of state has been applied.

3.4 Updated rate equation for vacancy flux

Another benefit of the improved description of the bubble pressure based on the new equation of state is that the driving force for grain boundary vacancy absorption by bubbles is better captured. We have also implemented a new equation for the rate of vacancy absorption based on a similar formulation that used in cluster dynamics, such as that described by Matthews et al. [32]. In this case, the reaction energy between a vacancy and bubble is described as a function of the deviation from the equilibrium bubble pressure and is used to define the driving force. Additionally, the pre-factor has been derived based on the grain boundary bubble intersecting the grain to create a cylindrical capture region with radius equal to that of the bubble and thickness equal to that of the grain boundary. The cylindrical assumption is based on the fact that the bubble radius is much larger than the grain boundary thickness. This is described in more detail in Section 2.4.2. The results using this new form of rate equation for vacancy absorption are shown in Fig. 3.4. Only small differences are seen compared to the previous linear assumption for this mechanism. Virtually no difference is seen in the outer periphery of the pellet as this mechanism is essentially completely inactive anyway due to the immobility of grain boundary vacancies at this temperature.

Nonetheless, we did notice that smoother increases in all three of n_{Xe}/n_v, pressure, and radius occur at the mid-point and inner regions of the pellet. We believe that this is because the new formulation, see Eq. (2.20), fairly quickly reaches a maximum value of $\frac{2\pi[v]D_v\delta}{\Omega \ln\left(\frac{R_c}{R}\right)}$ as the bubble pressure exceeds p_{eq}. This means that bubbles hit a steady growth rate that is limited by the self-diffusivity at the grain boundary, $[v]D_v$. The original linear approximation shown in Eq. (2.5) means that there is always feedback between the bubble pressure and the vacancy flux, which we could cause the jumps in bubble characteristics shown in Fig. 3.3, compared to the relatively smooth increase with the updated rate equation shown in Fig. 3.4.

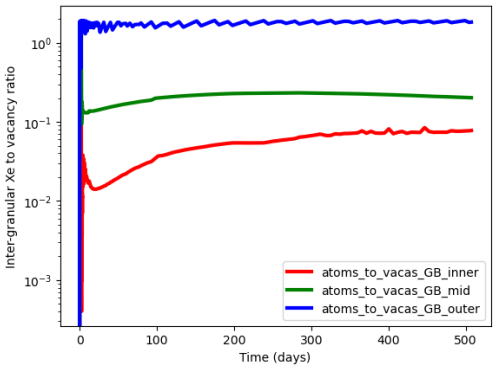

(a) $\frac{n_{Xe}}{n_{vaca}}$ ratio

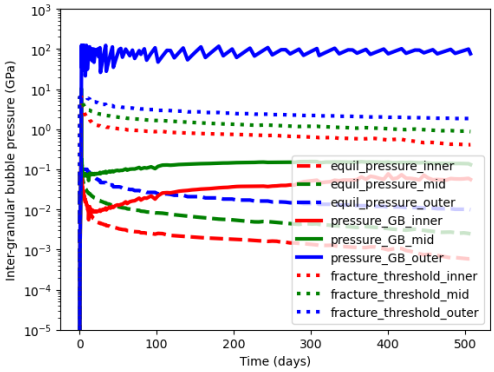

(b) Pressure

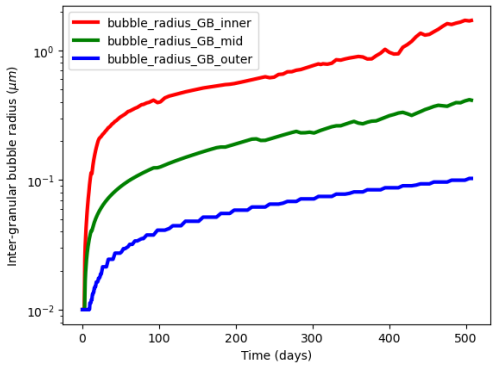

(c) Radius

Figure 3.4: Prediction from the SIFGRS model in BISON for inter-granular bubble behavior at three position in the fuel pellet for the IFA-677.1R5 case with a constant power applied. Updated vacancy flux rate equations have been applied.

3.5 Cracking added

It can be clearly seen in Fig. 3.4b that the bubble pressures in the periphery of the pellet are well in excess of the expected fracture threshold derived from MD. This is due to the low diffusivity of grain boundary vacancies at low temperature being insufficient to relieve bubble pressure. Therefore, we have implemented a cracking growth mechanism as described in Section 2.4.5.

Figure 3.5 shows the bubble n_{Xe}/n_v, pressure and radius as a function of time. The bubbles at the inner and mid points of the pellet are unaffected by the addition of this cracking mechanism. This is expected given that cracking can only be activated for bubble pressures that exceed the cracking threshold, which does not occur in these regions of the pellet.

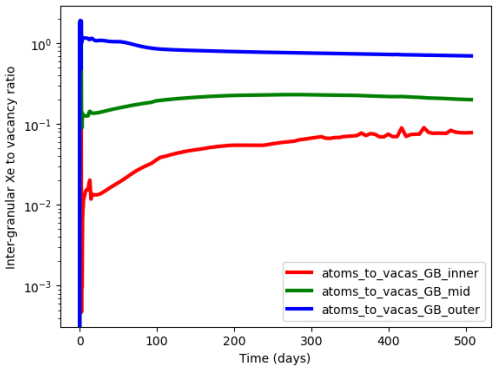

(a) $\frac{n_{Xe}}{n_{vaca}}$ ratio

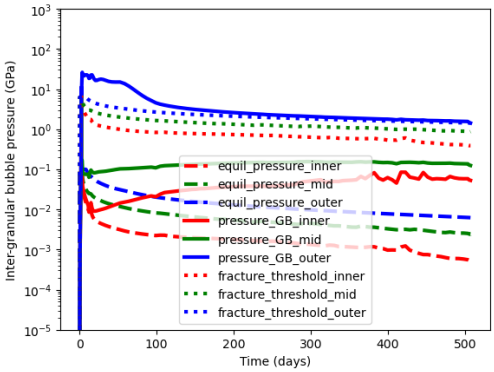

(b) Pressure

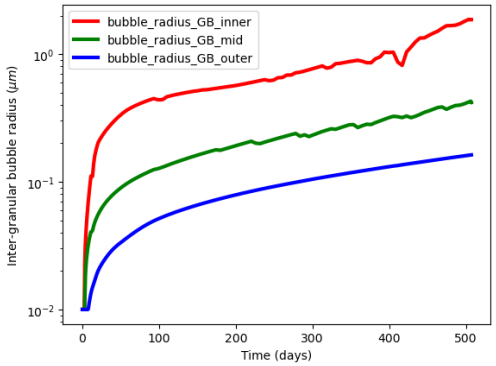

(c) Radius

Figure 3.5: Prediction from the SIFGRS model in BISON for inter-granular bubble behavior at three position in the fuel pellet for the IFA-677.1R5 case with a constant power applied. A cracking bubble growth mechanisms has been applied.

Figure 3.5a shows that in the periphery of the pellet n_{Xe}/n_v settles at about 0.9. This corresponds to a convergence of the bubble pressure to the fracture threshold, as shown in Fig. 3.5b, which is now the limiting mechanism for bubble pressure. Naturally there is a corresponding increase in the bubble radius, as can be been by comparing Fig. 3.5c with Fig. 3.4c. For example, at the end of the simulation the bubble radius in the periphery of the pellet now reaches 162 nm,

whereas without cracking enabled it only reached 102 nm.

One significant outcome of the outer bubble pressure being limited to the cracking threshold of about 3 GPa is that it ensures the bubble is in a regime of the equation of state where the bubble pressure is temperature dependent. This is a pre-requisite of a temperature transient being able to cause a rise in bubble pressure, which in turn is a pre-requisite for transient-induced micro-cracking or pulverization via a bubble mechanism. If the bubble pressure is at around 100 GPa, as is the case without micro-cracking growth during steady state (see Fig. 3.4b), the equation of state does not exhibit any temperature-dependence in the bubble pressure and could not contribute to a rise in bubble pressure during a transient. This highlights the importance of cracking as a growth mechanism even during steady-state. Next we will examine the response of the system to a temperature ramp.

3.6 Temperature transient

As a test, the same simulation was modified so that at 253 days the coolant inlet temperature was increased from 506 K to 1200 K over 1 minute. Simultaneously the power was dropped to zero. The objective of this exercise was to probe the qualitative response of the bubbles to something approximating LOCA conditions, rather than to do a true evaluation of a LOCA.

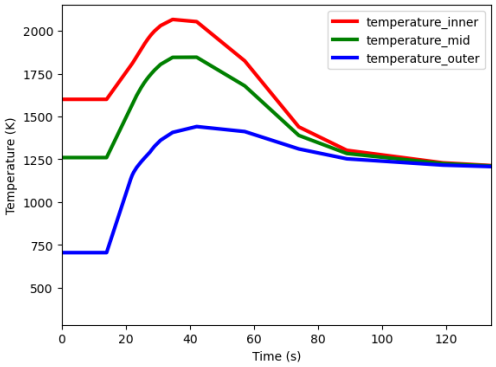

(a) Temperature

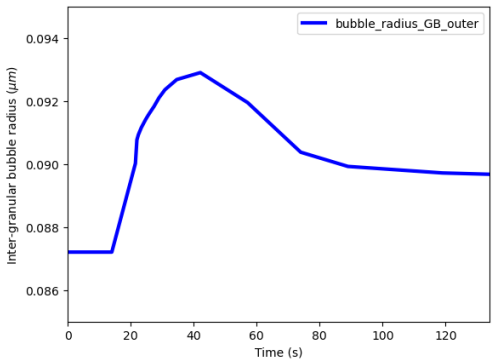

(b) Pressure

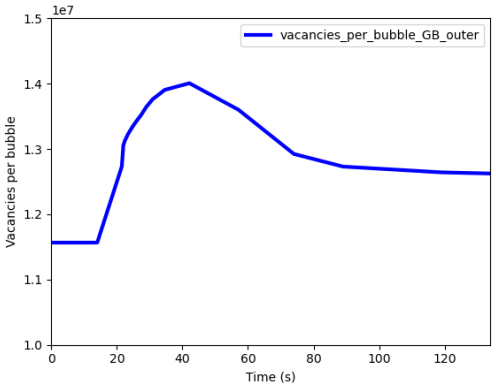

(c) Radius

Figure 3.6: Prediction from the fully modified SIFGRS model in BISON for inter-granular bubble behavior at three position in the fuel pellet for the IFA-677.1R5 case. Mock LOCA conditions were applied after 253 days.

Figure 3.6a shows the change in the temperature at different positions in the pellet. The initial rise in the temperature can be seen as the coolant temperature begins to increase. Following the initial rise, the temperature begins to fall as the power is shut off. Eventually all locations in the pellet settle on the new inlet temperature of 1200 K.

During the rise in temperature, there is an increase in the radius of the bubbles in the outer location of the pellet, see Fig. 3.6b. This is driven by an increase in the bubble pressure and an immediate corresponding increase in the volume to account for the cracking growth mechanism. The radius increases by about 5 nm. This is clearly insufficient to cause interconnection and transient fission gas release. For example, just before the deviation from steady-state, the bubble

areal density is 1.23 $\times 10^{13}$ m^{-2}, which approximately corresponds to a separation of bubble centers of 284 nm. Therefore, the bubble radius would need to reach half that (142 nm) for interconnection to occur.

However, as discussed previously, we have assumed that all of the volume needed to alleviate the pressure increase is evenly distributed within the bubble so that it maintains its shape. This assumption is based on surface diffusion occurring very rapidly and on shorter timescales than the other processes. This is an acceptable assumption for steady-state conditions; however, it may not be valid during a transient. On short timescales, it is more accurate to assumed the volume increase can be attributed to cylindrical cracks emanating from each bubble. If we assign the number of vacancies that the bubble must increase by to relieve the pressure (see Fig. 3.6c) entirely to six cylindrical cracks of radius 10 nm, the crack length would be 54 nm. At the beginning of the transient, the separation between the bubble surfaces is about 52 nm. Despite the significant assumptions that have been applied, this estimate indicates a promising path forward to mechanistically describe transient fission gas release and pulverization with a direct connection to the fission gas bubble evolution.

4 Future work

As discussed in the previous section, when we combine atomic scale informed models for i) a description of the diffusion mechanisms of fission gas to the bubbles, ii) a new equation of state, and iii) a fracture threshold for grain boundary bubbles, there is the potential for a mechanistic understanding of how micro-cracking occurs and can lead to bubble interconnection during a transient. For complete implementation of such a description, the model must be extended to allow cracks to propagate on short timescale and several assumptions must be tested:

- If the fracture threshold is exceeded, rather than assign the volume needed to relieve bubble pressure evenly to the whole bubble volume (allowing it to maintain its shape), we should assign that volume to cracks that protrude from the bubble. A rate equation will be implemented that will then allow the crack volume to be reassigned to the bubble volume based on the diffusion of vacancies along the bubble surface. It is expected that this rate equation will allow cracks to grow on short (transient) timescales but on longer timescales they will not be able to grow fast enough before they become incorporated into the main bubble volume and shrink. During the transient or LOCA, if the cracks are longer than the distance between bubbles, they will be considered interconnected and will result in fission gas release.
- The cross-sectional area of the crack will impact their length during a transient. The crack geometry should be investigated using MD simulations that are currently on-going in a separate milestone.
- The number of cracks per bubble and the arrangement of bubbles on a grain boundary surface is not well known and should be studied using either MD or phase field simulations, or some combination of both.
- Any temperature dependence in the MD-informed fracture threshold should be studied.
- Dislocation punching has been omitted from this study. However, the bubbles in the outer region of the pellet do exceed the pressure needed for the onset of dislocation punching. We have assumed in this work (based on the creep rates begin extremely low in UO_2 at these temperatures) that dislocation punching does not occur. However, further work should be done to either revise or justify this assumption. It is possible that dislocation punching could reduce bubble pressures during steady-state operation.
- Nothing in this model so far accounts for the change in microstructure associated with the formation of high burnup structure. Efforts at INL to understand HBS formation and implement those findings in BISON are on-going. Ultimately, these models should be integrated to allow a better description of pulverization.

- Both micro-cracking, which contributes to transient fission gas release throughout the lifetime of the fuel, and complete grain boundary fracture leading to pulverization are thought to be associated with the thermal expansion of over-pressurized bubbles during a temperature excursions. Future development of this model should seek to resolve differences between these phenomena and, where appropriate, identify common underlying mechanisms.

The above points are beyond the scope of this milestone but should form the basis of future work to develop and implement a mechanistic model of pulverization and transient fission gas release. Efforts at INL and LANL are continuing to investigate this behavior at different length scales and can be coordinated to address some of the points suggested here for future work.

5 Conclusions

Results from atomic scale simulations and cluster dynamics simulations have been implemented in the fuel performance code BISON. As shown previously, the over pressurization of bubbles reduces the driving force for Xe interstitials to arrive at grain boundary bubbles as Xe to vacancy reaches 2:1. However, the previous equation of state and assumptions regarding the bubble volume were insufficient to describe the bubble pressures and radii in the cooler periphery of the pellet. To address this, a new equation of state from Yang and Wirth was implemented, as was the fracture threshold from Galvin et al.. Both of these models were derived from MD simulations.

The new equation of state allowed a better prediction of bubble pressures, which allowed the fracture threshold as a function of radius to be used to indicate the onset of micro-cracks. We have assumed that bubbles can grow via this fracture mechanism and that the cracks are immediately reincorporated in to the main bubble volume. This became the dominant growth mechanism for bubbles in the outer region of the pellet under steady state conditions. When a temperature transient was applied after 253 days, we found that the growth in bubble radius through cracking was insufficient to allow interconnection of bubbles and release of gas.

However, if one assumes that cracks cannot be incorporated back into the bubbles on short timescales and instead protrude from the bubbles, it appears that it is possible for cracks to interconnect. This may be able to explain transient fission gas release and potentially pulverization. A significant number of assumptions still need to be tested and a time dependent crack growth/shrinkage model implemented before final conclusions can be made, but a path forward to achieve this has been proposed.

Acknowledgments

Funding for this work was provided by the US Department of Energy, Office of Nuclear Energy NEAMS (Nuclear Energy Advanced Modeling and Simulation) program. Los Alamos National Laboratory, an affirmative action/equal opportunity employer, is operated by Triad National Security LLC, for the National Nuclear Security Administration of the U.S. Department of Energy under Contract No. 89233218CNA000001.

References

[1] Michael WD Cooper, Christopher Matthews, and David A. Andersson. Informing fuel performance through simulations of irradiation-enhanced diffusion in ceramic nuclear fuels: LA-UR-22-23945. Technical report, LANL, Los Alamos, USA, 2022.

[2] L. Yang and B. D. Wirth. An improved xenon equation of state for nanobubbles in UO_2. *Journal of Nuclear Materials*, 572:154089, 2022.

[3] COT Galvin, David A. Andersson, and Michael W.D. Cooper. Development of fracture criteria for UO2 HBS grain boundaries from atomic scale simulation data for use in meso-scale simulations: LA-UR-22-29943. Technical report, LANL, Los Alamos, USA, 2022.

[4] Vincenzo V. Rondinella and Thierry Wiss. The high burn-up structure in nuclear fuel. *Materials Today*, 13(12):24–32, 2010.

[5] K. Nogita and K. Une. Irradiation-induced recrystallization in high burnup UO_2 fuel. *Journal of Nuclear Materials*, 226(3):302–310, 1995.

[6] K. Nogita and K. Une. Radiation-induced microstructural change in high burnup UO_2 fuel pellets. *Nuclear Inst. and Methods in Physics Research, B*, 91(1-4):301–306, 1994.

[7] K. Une, K. Nogita, S. Kashibe, and M. Imamura. Microstructural change and its influence on fission gas release in high burnup UO_2 fuel. *Journal of Nuclear Materials*, 188(C):65–72, 1992.

[8] T. Sonoda, M. Kinoshita, I. L.F. Ray, T. Wiss, H. Thiele, D. Pellottiero, V. V. Rondinella, and Hj Matzke. Transmission electron microscopy observation on irradiation-induced microstructural evolution in high burn-up UO2 disk fuel. *Nuclear Instruments and Methods in Physics Research, Section B: Beam Interactions with Materials and Atoms*, 191(1-4):622–628, 2002.

[9] T. Wiss, H. Thiele, A. Janssen, D. Papaioannou, V. V. Rondinella, and R. J.M. Konings. Recent results of microstructural characterization of irradiated light water reactor fuels using scanning and transmission electron microscopy. *Journal of Materials*, 64(12):1390–1395, 2012.

[10] M. Kinoshita, T. Kameyama, S. Kitajima, and Hj Matzke. Temperature and fission rate effects on the rim structure formation in a UO_2 fuel with a burnup of 7.9% FIMA. *Journal of Nuclear Materials*, 252(1-2):71–78, 1998.

[11] N. Lozano, L. Desgranges, D. Aymes, and J. C. Niepce. High magnification SEM observations for two types of granularity in a high burnup PWR fuel rim. *Journal of Nuclear Materials*, 257(1):78–87, 1998.

[12] I. L.F. Ray, Hj. Matzke, H. Thiele, and M. Kinoshita. An electron microscopy study of the RIM structure of a UO_2 fuel with a high burnup of 7.9% FIMA. *Journal of Nuclear Materials*, 245:115–123, 1997.

[13] C. T. Walker, D. Staicu, M. Sheindlin, D. Papaioannou, W. Goll, and F. Sontheimer. On the thermal conductivity of UO_2 nuclear fuel at a high burn-up of around 100 MWd/kgHM. *Journal of Nuclear Materials*, 350(1):19–39, 2006.

[14] Clive Walker. Electron probe microanalysis of irradiated nuclear fuel: An overview. *Journal of analytical atomic spectrometry*, 14(3):447–454, 1999.

[15] Xian Ming Bai, Michael R. Tonks, Yongfeng Zhang, and Jason D. Hales. Multiscale modeling of thermal conductivity of high burnup structures in UO_2 fuels. *Journal of Nuclear Materials*, 470:208–215, mar 2016.

[16] J. A. Turnbull, S. K. Yagnik, M. Hirai, D. M. Staicu, and C. T. Walkert. An assessment of the fuel pulverization threshold during LOCA-type temperature transients. *Nuclear Science and Engineering*, 179(4):477–485, 2015.

[17] R. A. Jackson and C. R.A. Catlow. Trapping and solution of fission Xe in UO_2. Part 2. Solution from small overpressurized bubbles. *Journal of Nuclear Materials*, 127(2-3):167–169, 1985.

[18] X. Y. Liu, B. P. Uberuaga, D. A. Andersson, C. R. Stanek, and K. E. Sickafus. Mechanism for transient migration of xenon in UO_2. *Applied Physics Letters*, 98(15), 2011.

[19] Alexander E. Thompson and C. Wolverton. First-principles study of noble gas impurities and defects in UO_2. *Physical Review B - Condensed Matter and Materials Physics*, 84(13):1–11, 2011.

[20] D. A. Andersson, P. Garcia, X. Y. Liu, G. Pastore, M. Tonks, P. Millett, B. Dorado, D. R. Gaston, D. Andrs, R. L. Williamson, R. C. Martineau, B. P. Uberuaga, and C. R. Stanek. Atomistic modeling of intrinsic and radiation-enhanced fission gas (Xe) diffusion in $UO_{2\pm x}$: Implications for nuclear fuel performance modeling. *Journal of Nuclear Materials*, 451(1-3):225–242, 2014.

[21] David A. Andersson, Michael R. Tonks, Luis Casillas, Shyam Vyas, Pankaj Nerikar, Blas P. Uberuaga, and Christopher R. Stanek. Multiscale simulation of xenon diffusion and grain boundary segregation in UO_2. *Journal of Nuclear Materials*, 462:15–25, 2015.

[22] Emerson Vathonne, David A. Andersson, Michel Freyss, Romain Perriot, Michael W.D. Cooper, Christopher R. Stanek, and Marjorie Bertolus. Determination of Krypton Diffusion Coefficients in Uranium Dioxide Using Atomic Scale Calculations. *Inorganic Chemistry*, 56(1):125–137, 2017.

[23] D. A. Andersson, B. P. Uberuaga, P. V. Nerikar, C. Unal, and C. R. Stanek. U and Xe transport in $UO_{2\pm x}$: Density functional theory calculations. *Physical Review B - Condensed Matter and Materials Physics*, 84(5):1–12, 2011.

[24] Romain Perriot, Christopher Matthews, Michael W.D. Cooper, Blas P. Uberuaga, Christopher R. Stanek, and David A. Andersson. Atomistic modeling of out-of-pile xenon diffusion by vacancy clusters in UO_2. *Journal of Nuclear Materials*, 520:96–109, 2019.

[25] C. R. A. Catlow. Theory of fission gas migration in UO_2. *Radiation Effects*, 53(3-4):127–132, 1980.

[26] M. Huang, D. Schwen, and R. S. Averback. Molecular dynamic simulation of fission fragment induced thermal spikes in UO_2: Sputtering and bubble re-solution. *Journal of Nuclear Materials*, 399(2-3):175–180, 2010.

[27] K. Govers, C. L. Bishop, D. C. Parfitt, S. E. Lemehov, M. Verwerft, and R. W. Grimes. Molecular dynamics study of Xe bubble re-solution in UO_2. *Journal of Nuclear Materials*, 420(1-3):282–290, 2012.

[28] Wahyu Setyawan, Michael W.D. Cooper, Kenneth J. Roche, Richard J. Kurtz, Blas P. Uberuaga, David A. Andersson, and Brian D. Wirth. Atomistic model of xenon gas bubble re-solution rate due to thermal spike in uranium oxide. *Journal of Applied Physics*, 124(7), 2018.

[29] X. Y. Liu and D. A. Andersson. Molecular dynamics study of fission gas bubble nucleation in UO_2. *Journal of Nuclear Materials*, 462:8–14, 2015.

[30] S. T. Murphy, A. Chartier, L. Van Brutzel, and J. P. Crocombette. Free energy of Xe incorporation at point defects and in nanovoids and bubbles in UO_2. *Physical Review B - Condensed Matter and Materials Physics*, 85(14):1–9, 2012.

[31] Samuel T. Murphy, Paul Fossati, and Robin W. Grimes. Xe diffusion and bubble nucleation around edge dislocations in UO_2. *Journal of Nuclear Materials*, 466:634–637, 2015.

[32] Christopher Matthews, Romain Perriot, Michael W.D. Cooper, Christopher R. Stanek, and David A. Andersson. Cluster dynamics simulation of uranium self-diffusion during irradiation in UO_2. *Journal of Nuclear Materials*, 527:151787, dec 2019.

[33] Christopher Matthews, Romain Perriot, Michael W.D. Cooper, Christopher R. Stanek, and David A. Andersson. Cluster dynamics simulation of xenon diffusion during irradiation in UO_2. *Journal of Nuclear Materials*, 540:152326, nov 2020.

[34] Michael W.D. Cooper, Christopher Matthews, and David A. Andersson. Investigating bubble pressures in irradiated UO_2 for understanding fragmentation of high burnup structure. Technical report, LANL LA-UR-20-27793, 2020.

[35] David A. Andersson and Michael W.D. Cooper. Fuel Pulverization During Temperature Ramps: Molecular Dynamics Simulations. Technical report, EPRI: https://www.epri.com/research/products/000000003002020945, 2021.

[36] Michael W.D. Cooper, Christopher Matthews, and David A. Andersson. Gas evoluitonin high-burnup fuel and its impact on fuel fragmentation. Technical report, Los Alamos National Laboratory, Los Alamos, USA, 2021.

[37] Radomir Josek. The high initial rating test IFA- 677.1: Final report on in-pile results, HWR-872. Technical report, Organisation for Economic Co-operation and Development Halden Reactor Project, Halden, Norway, 2008.

[38] Jakob Arborelius, Karin Backman, Lars Hallstadius, Magnus Limbäck, Jimmy Nilsson, Björn Rebensdorff, Gang Zhou, Koji Kitano, Reidar Löfström, and Gunnar Rönnberg. Advanced doped UO2 pellets in LWR applications. *Journal of Nuclear Science and Technology*, 43(9):967–976, 2006.

[39] Taku Watanabe, Susan B. Sinnott, James S. Tulenko, Robin W. Grimes, Patrick K. Schelling, and Simon R. Phillpot. Thermal transport properties of uranium dioxide by molecular dynamics simulations. *Journal of Nuclear Materials*, 375(3):388–396, apr 2008.

[40] Jason D. Hales, Richard L. Williamson, Stephen R. Novascone, Giovanni Pastore, Benjamin W. Spencer, D. S. Stafford, Kyle A. Gamble, Danielle M. Perez, Russell J. Gardner, W. Liu, J. Galloway, Christopher Matthews, C. Unal, and N. Carlson. BISON Theory Manual The Equations Behind Nuclear Fuel Analysis, INL/EXT-13-29930 Rev. 3. Technical Report September, Idaho National Laboratory, Idaho Falls, USA, 2013.

[41] D. D. Lanning, C. E. Beyer, and K. J. Geelhood. FRAPCON-3 Updates, Including Mixed-Oxide Fuel Properties. NUREG/CR-6534, Vol. 4 PNNL-11513. Technical report, Pacific Northwest National Laboratory, Richmod, USA, 2005.

[42] J K Fink. Thermophysical properties of uranium dioxide. *Journal of Nuclear Materials*, 279:1–18, 2000.

[43] C. M. Allison, G. A. Berna, R. Chambers, E. W. Coryell, K. L. Davis, D. L. Hagrman, D. T. Hagrman, N. L. Hampton, and J. K. Hohorst. SCDAP/RELAP5/MOD3.1 code manual, volume IV: MATPRO—A library of materials properties for light-water-reactor accident analysis. NUREG/CR-6150, EGG-2720. Technical report, Idaho National Laboratory, Idaho Falls, USA, 1993.

[44] J. B. Ainscough, B. W. Oldfield, and J. O. Ware. Isothermal grain growth kinetics in sintered UO_2 pellets. *Journal of Nuclear Materials*, 49(2):117–128, 1973.

[45] Terje Tverberg. Update on the in-pile results from the fission as release mechanisms study in IFA-716, HWR-1090. Technical report, Organisation for Economic Co-operation and Development Halden Reactor Project, Halden, Norway, 2014.

[46] Y. Rashid, R. Dunham, and R. Montgomery. Fuel analysis and licensing code: FAL- CON MOD01, EPRI 1011308. Technical report, EPRI, 2004.

[47] Masaomi Oguma. Microstructure effects on fracture strength of UO_2 fuel pellets. *Journal of Nuclear Science and Technology*, 19(12):1005–1014, 1982.

[48] T. Barani, D. Pizzocri, G. Pastore, L. Luzzi, and J. D. Hales. Isotropic softening model for fuel cracking in BISON. *Nuclear Engineering and Design*, 342(September 2018):257–263, 2019.

[49] Richard L. Williamson, Jason D. Hales, Stephen R. Novascone, Giovanni Pastore, Kyle A. Gamble, Benjamin W. Spencer, Wen Jiang, Stephanie A. Pitts, Albert Casagranda, Daniel Schwen, Adam X. Zabriskie, Aysenur Toptan, Russell Gardner, Christoper Matthews, Wenfeng Liu, and Hailong Chen. BISON: A Flexible Code for Advanced Simulation of the Performance of Multiple Nuclear Fuel Forms. *Nuclear Technology*, 207(7):954–980, 2021.

[50] Giovanni Pastore, Lelio Luzzi, Valentino Di Marcello, and Paul Van Uffelen. Physics-based modelling of fission gas swelling and release in UO_2 applied to integral fuel rod analysis. *Nuclear Engineering and Design*, 256:75–86, 2013.

[51] M. V. Speight. A Calculation on the Migration of Fission Gas in Material Exhibiting Precipitation and Re-solution of Gas Atoms Under Irradiation. *Nuclear Science and Engineering*, 37(2):180–185, 1969.

[52] Frank S. Ham. Theory of diffusion-limited precipitation. *Journal of Physics and Chemistry of Solids*, 6(4):335–351, 1958.

[53] R. J. White and M. O. Tucker. A new fission-gas release model. *Journal of Nuclear Materials*, 118(1):1–38, 1983.

[54] D. Pizzocri, G. Pastore, T. Barani, A. Magni, L. Luzzi, P. Van Uffelen, S. A. Pitts, A. Alfonsi, and J. D. Hales. A model describing intra-granular fission gas behaviour in oxide fuel for advanced engineering tools. *Journal of Nuclear Materials*, 502:323–330, 2018.

[55] Michael WD Cooper, Giovanni Pastore, Yifeng Che, Christopher Matthews, Axel Forslund, Christopher R. Stanek, Koroush Shirvan, Terje Tverberg, Kyle A. Gamble, Brian Mays, and David A. Andersson. Fission gas diffusion and release for Cr_2O_3-doped UO_2: From the atomic to the engineering scale. *Journal of Nuclear Materials*, 545:152590, mar 2021.

[56] J A Turnbull, C A Friskney, J R Findlay, F A Johnson, and A J Walter. The Diffusion Coefficients of Gaseous and Volatile Species during the Irradiation of Uranium Dioxide. *Journal of Nuclear Materials*, 107:168–184, 1982.

[57] J A Turnbull, R J White, and C Wise. The Diffusion Coefficients for Fission Gas Atoms in Uranium Dioxide. In *Water Reactor Fuel Element Computer Modeling in Steady State, Transient and Accident Conditions Proceedings of a Technical Committee Meeting Organized by the International Atomic Energy Agency and Held in Preston*, pages 174–181, Preston, UK, 1989.

[58] S Kashibe, K Une, and K Nogita. Formation and growth of intragranular fuels with burnup of 6-83 GWd/t fission gas bubbles in UO_2. *Journal of Nuclear Materials*, 206:22–34, 1993.

[59] Giovanni Pastore, L. P. Swiler, J. D. Hales, S. R. Novascone, D. M. Perez, B. W. Spencer, L. Luzzi, P. Van Uffelen, and R. L. Williamson. Uncertainty and sensitivity analysis of fission gas behavior in engineering-scale fuel modeling. *Journal of Nuclear Materials*, 456:398–408, 2015.

[60] M. V. Speight and W. Beere. Vacancy Potential and Void Growth on Grain Boundaries. *Met Sci J*, 9(4):190–191, 1975.

[61] Aaron A. Kohnert and Laurent Capolungo. Sink strength and dislocation bias of three-dimensional microstructures. *Physical Review Materials*, 3(5):1–12, 2019.

[62] Donald R Olander. *Fundamental aspects of nuclear reactor fuel elements*. Springfield, Viginia, 1976.